Research Square

Preprints are preliminary reports that have not undergone peer review.
They should not be considered conclusive, used to inform clinical practice,
or referenced by the media as validated information.

Zhuhong Ointment Improves Infected Diabetic Wounds via CK2-βTrCP-SUN2 Protein Network

Xue Li
Beijing Hospital of Traditional Chinese Medicine
Xinran Xie
Beijing Hospital of Traditional Chinese Medicine
Zhongwu Zhou
Beijing Hospital of Traditional Chinese Medicine
Xiujuan He
Beijing Hospital of Traditional Chinese Medicine
Ling Han
Jianqiao Liu
Beijing Hospital of Traditional Chinese Medicine
Yu Lu
Beijing Hospital of Traditional Chinese Medicine
Zihao Liu
Beijing Hospital of Traditional Chinese Medicine
Jindong Zheng
Yipeng Chai
Yudong Li
liyudong@bjzhongyi.com

Beijing Hospital of Traditional Chinese Medicine

Article

Keywords: Zhuhong Ointment, diabetic infected cutaneous wound, macrophage polarization, CK2-βTrCP-SUN2 protein network

Posted Date: November 18th, 2026

DOI: https://doi.org/10.21203/rs.3.rs-11768455/v1

License: This work is licensed under a Creative Commons Attribution 4.0 International License.
Read Full License

Additional Declarations: No competing interests reported.

Zhuhong Ointment Improves Infected Diabetic Wounds via CK2-βTrCP-SUN2 Protein Network

Xue Li[a], Xinran Xie[a,b], Zhongwu Zhou[a], Xiujuan He[a,b], Ling Han[c], Jianqiao Liu[a], Yu Lu[a], Zihao Liu[a], Jindong Zheng[d], Yipeng Chai[e], Yudong Li[*]

[a]Department of Coloproctology, Beijing Hospital of Traditional Chinese Medicine, Capital Medical University，Beijing，China

[b]Beijing Institute of Traditional Chinese Medicine, Beijing,China

[c]Xining No.2 People's Hospital, Xining City, Qinghai Province, China

[d]Department of Coloproctology, Changzhi Traditional Chinese Medicine Hospital，Shanxi Province，China

[e]Department of Coloproctology, Changzhi Traditional Chinese Medicine Hospital，Shanxi Province，China

*Correspondence: Department of Coloproctology, Beijing Hospital of Traditional Chinese Medicine, Capital Medical University，Beijing，China. No. 23rdArt Museum Back Street, Dongcheng District, Beijing 100010, China. E-mail:liyudong@bjzhongyi.com

Abstract

Purpose : Wounds after anal fistula surgery readily develop into refractory wounds due to hyperglycemia and persistent chronic inflammation, and current clinical therapies lack effective strategies targeting the inflammatory microenvironment. Imbalanced M1/M2 macrophage polarization is critical for delayed wound healing. The CK2-βTrCP-SUN2 pathway participates in macrophage polarization regulation, yet its drug-modulated mechanism in diabetic infected wounds remains unclear. Zhuhong Ointment (ZHO) clinically repairs chronic ulcers, though its molecular mechanism is poorly defined.This study aims to investigate ZHO's therapeutic effect on diabetic infected wounds and clarify whether it modulates macrophage polarization via the CK2-βTrCP-SUN2 network.

Materials and methods： A refractory wound model was established in db/db mice with multiple groups for wound and inflammation evaluation. LPS+IFN-γ induced M1 macrophages in vitro. Flow cytometry, CoIP and CK2 intervention were used to verify polarization, nuclear morphology and SUN2 ubiquitination.

Results: ZHO accelerated wound healing, promoted collagen deposition and epidermal regeneration without affecting blood glucose, inhibited pro-inflammatory factors and promoted M2 polarization. It regulated CK2-βTrCP-SUN2 expression, improved nuclear abnormality, and promoted SUN2 ubiquitination. CK2 activation reversed ZHO effects, while inhibition mimicked them.

Conclusion: ZHO balances macrophage polarization via the CK2-βTrCP-SUN2 network, relieves chronic inflammation and promotes tissue repair, providing potential targets for treating diabetic infected wounds.

Key words: Zhuhong Ointment; diabetic infected cutaneous wound; macrophage polarization; CK2-βTrCP-SUN2 protein network

1. Introduction

Wounds after anal fistula surgery are prone to develop into refractory wounds due to high glucose stimulation, chronic inflammation and abnormal tissue repair function, often presenting as unhealed wounds, recurrent infection, slow granulation growth and disordered collagen metabolism, which seriously affect patients' quality of life and increase medical burden [1–3]. Current clinical treatments mostly adopt symptomatic treatments such as debridement, anti-infection and improving microcirculation, lacking effective schemes targeting the regulation of inflammatory microenvironment and repair pathways [4,5]. Therefore, exploring the core molecular mechanisms and screening effective intervention targets and drugs have important clinical significance and translational value.

Macrophages are the core regulatory cells of the wound immune microenvironment, and the dynamic transformation of their polarization phenotype is the key to determining inflammation resolution and tissue repair prognosis [6,7]. During normal wound repair, macrophages can complete an orderly transition from the pro-inflammatory M1 phenotype to the reparative M2 phenotype [8]；The pathological environment after anal fistula surgery can lead to macrophages remaining continuously in the M1 activated state, secreting large amounts of pro-inflammatory factors such as TNF-α, IL-1β and IL-6, resulting in persistent wound inflammation, impaired repair cell function and extracellular matrix remodeling disorder, ultimately forming refractory wounds [9,10]. Therefore, targeted regulation of macrophage polarization balance is a core strategy to improve chronic inflammation and remodeling repair function of difficult-to-heal wounds after anal fistula surgery.

Existing studies have confirmed that nuclear membrane structure and nucleoskeleton proteins are involved in the regulation of macrophage polarization [11,12]. Among them, abnormal high expression of nuclear membrane key proteins SUN2 can induce nuclear morphological distortion and contraction, promoting M1 macrophage polarization [13]. Existing literature demonstrates that CK2 kinase and E3 ubiquitin ligase βTrCP jointly participate in the phosphorylation and ubiquitin-dependent degradation of SUN2 protein [14,15]，it is suggested that the CK2-βTrCP-SUN2 signaling axis is an important molecular pathway regulating macrophage polarization and chronic inflammation, but the role of this pathway in difficult-to-heal wounds after anal fistula surgery and its drug regulation mechanism remain unclear.

ZHO is an in-hospital preparation of Beijing Traditional Chinese Medicine

Hospital, used to treat chronic ulcers and long-term non-healing ulcers. It can effectively resist infection, promote granulation tissue proliferation and accelerate wound repair clinically, but its underlying molecular mechanism has not been clarified [16–18]. Previous studies have demonstrated that ZHO causes no obvious damage to the liver and kidneys at conventional doses. However, long-term and excessive administration leads to mercury accumulation in the liver, kidneys and brain, thereby inducing hepatic and renal toxicity[19]. Diabetic anal fistula postoperative wounds are hard to heal due to hyperglycemia, repeated faecal contamination and dysregulated macrophage polarization. This study used infected skin wound model of db/db diabetic mice to explore ZHO's efficacy and its correlation with the CK2-βTrCP-SUN2 protein network.

2. Materials and Methods

2.1. Animal Experiments

Male 12-week-old SPF db/db mice (C57BL/6J background) were used in this study. All mice were purchased from Beijing Vital River Laboratory Animal Technology Co., Ltd. The experimental animals were raised in a standardized animal room with ambient temperature controlled at (22±2) °C, relative humidity (50±5) %, and a 12-hour light/dark cycle. Mice had free access to standard rodent feed and sterile drinking water, and were acclimated for 1 week before the formal experiment. This experiment was approved by the Animal Welfare Ethics Committee of Beijing MDKN Biotechnology Co., Ltd., and strictly carried out in accordance with the Guide for the Care and Use of Laboratory Animals of the Beijing Municipal Bureau of Animal Health.

2.2. Animal Model Establishment

This study constructed full-thickness infected cutaneous wounds on the back of db/db diabetic mice. This model reproduces the core pathological features of refractory wounds after anal fistula surgery in diabetic patients, including hyperglycemic background and persistent fecal bacterial stimulation, and avoids the technical difficulty of stable anal fistula modeling in small rodents. The modeling method was referred to reference[20,21]. After anesthesia with intraperitoneal injection of pentobarbital sodium (80 mg/kg), the mid-back of the mice was depilated with an area of 4 cm×4 cm. A wound with an area of 3 cm×3 cm was cut on the back with surgical scissors, destroying the full-thickness skin and superficial subcutaneous fascia up to the muscular layer. After 24 hours of compression hemostasis with gauze bandage, the dressing was removed, and each mouse was raised in a single cage. The model group (db/db mice) was

uniformly sprayed with 1 mL fecal suspension (1 g/mL mouse feces, prepared with normal saline, freshly prepared) on the wound site daily. Successful modeling was confirmed at 72 hours by purulent secretion, excessive exudate and redness of the wound margin.

2.3. Drug Preparation

Vermilion Ointment Gauze Strips: Composed of cinnabar, red mercuric oxide and petrolatum. Every 100 grams of petrolatum contains 19 grams of 80-mesh crude drugs, which are evenly spread on gauze strips. Each square centimeter of the gauze strip carries 18 milligrams of ointment, with a crude drug content of 3.4 milligrams. The drug concentration of the high-dose group is 3.4 mg/cm² (equivalent to the clinical equivalent dose), the medium-dose group is 2 mg/cm², and the low-dose group is 1.2 mg/cm². The preparations are sterilized by high-pressure steam before use, and are produced and quality-controlled by the Preparation Room of Beijing Hospital of Traditional Chinese Medicine.

2.4. Experimental Grouping and Administration Methods

Model mice were randomly divided into six groups: model group, low-dose Vermilion Ointment group, medium-dose Vermilion Ointment group, high-dose Vermilion Ointment group, petrolatum ointment group and mupirocin ointment group. After successful modeling, 1 mL of distilled water was dripped onto the wound surface of mice in the blank control group every day, while 1 mL of fecal suspension was applied to the wound of mice in all other groups. Dressing change was performed 2 hours later. Before dressing change, the wound surface was cleaned with iodophor. Mice in the model group were applied with sterile gauze strips matching the size of the wound; mice in each Vermilion Ointment dose group were treated with gauze strips coated with Vermilion Ointment of corresponding concentrations; the petrolatum ointment group received petrolatum ointment gauze strips, and the mupirocin ointment group was given gauze strips coated with mupirocin ointment. Photographs were taken and wound area was measured to evaluate wound healing.

On the 14th day after administration, mice were anesthetized with pentobarbital. Blood was collected from the abdominal aorta, centrifuged at 3500 revolutions per minute for 10 minutes, and the supernatant serum was collected and stored at -80 ℃. Wound tissues on the back were harvested. Part of the tissues were fixed in 10% formaldehyde for paraffin section preparation, and the rest were embedded with OCT compound for frozen section preparation.

2.5. Reagent Sources

Total RNA Extraction Kit purchased from EZ-Bio（M5102）；HiScript II Reverse Transcriptase First Strand cDNA Synthesis Kit purchased from Vazyme（R223）；BCA Protein Quantitation Kit: purchased from Beyotime Biotechnology（P0010）；iNOS Antibody purchased from Proteintech（18985-1-AP）；Arg-1 Antibody purchased from Proteintech（16001-1-AP）；CCK-8 Cell Counting Kit purchased from DoJinDo（CK04）；SUN2 Antibody purchased from Proteintech（27556-1-AP）；LAminA/C Antibody purchased from Abcam（ab238303）；594-conjugated AffiniPure Donkey Anti-Rabbit IgG(H+L) purchased from Jackson（711-585-152 ）；488-conjugated AffininPure Goat Anti-Mouse IgG(H+L) purchased from Jackson（15-545-003）；FITC anti-mouse CD68 Antibody purchased from BioLegend（137005）；FITC anti-mouse CD206 (MMR) Antibody purchased from BioLegend（141703）；PE anti-mouse F4/80 Antibody purchased from BioLegend（111603）；CK2 Antibody purchased from Proteintech（21725-1-AP）；BTrCP Antibody purchased from Proteintech（28393-1-AP）；SUN1 Antibody purchased from abcam（Ab323868）；SUN2 Antibody purchased from Affinity（DF8403）。

2.6. H&E Staining

Wound tissues were paraffin-embedded into 4 μm sections after fixation. HE staining was performed, followed by microscopic observation of tissue repair and inflammation. Image analysis software is Slide Viewer.

2.7. Masson Staining

Paraffin sections were dewaxed to water, stained with hematoxylin for 5 min, and rinsed with running water to blue. Masson staining solution was used for sequential staining, phosphomolybdic acid differentiation, aniline blue staining for 5 min. Treated with 1% glacial acetic acid, gradient dehydration and clearing, neutral balsam sealing. Collagen fiber deposition and arrangement were observed under a light microscope, and collagen positive area was quantitatively analyzed by ImageJ (CVF (%) = (Collagen-positive area / Total tissue area) × 100%).

2.8. Western blot

Total protein was extracted from tissues or cells, quantified by BCA, separated by SDS-PAGE electrophoresis, and transferred to PVDF membrane. The membrane was blocked with 5% skimmed milk for 1 h. Primary antibody was incubated overnight at 4 °C, secondary antibody was incubated at room temperature for 1 h, ECL chemiluminescence development, and gray value was

quantified by ImageJ.

2.9. Flow Cytometry

Cell samples were collected from all experimental groups and thoroughly rinsed with cold PBS to remove impurities. Subsequently, cells were stained with fluorescent-conjugated CD86 and CD206 antibodies. The staining reaction was carried out for 30 minutes at room temperature under dark conditions to avoid fluorescence quenching. Finally, flow cytometry was used for detection and analysis. The proportion of $CD86^+$ cells reflected the percentage of M1 macrophages, and $CD206^+$ cells represented the proportion of M2 macrophages.

2.10. Immunofluorescence

Slides were fixed with 4% paraformaldehyde, permeabilized and blocked, then incubated with SUN2 primary antibody and Lamin A/C primary antibody overnight at 4 °C, and incubated with fluorescent secondary antibody in the dark for 1 h. Nuclei were stained with DAPI. Images were collected by laser confocal microscopy to analyze SUN2 expression, localization, nuclear contraction, nuclear morphology and nuclear area.

2.11. Co-Immunoprecipitation (Co-IP)

Cells were lysed with IP lysis buffer on ice, centrifuged, and supernatants harvested. A portion served as Input control. The rest was incubated with primary antibody overnight at 4 °C, followed by Protein A/G beads. After washing and boiling denaturation, samples were analyzed via Western blot.

2.12. Statistical Analysis

All data were expressed as mean ± SD, and analyzed by GraphPad Prism software 10.1. One-way analysis of variance (ANOVA) was used for comparison among multiple groups, and $P < 0.05$ was considered statistically significant.

3. Results

3.1. ZHO Improves Pathological Damage and Accelerates Wound Healing in db/db Mice

To investigate the overall pharmacological efficacy and tissue repair effects of ZHO on wound lesions after anal fistula surgery, a pharmacological evaluation was performed in animal models. Dynamic observation of wound healing revealed that ZHO effectively promoted wound contraction and markedly

accelerated the wound healing rate in a time-dependent manner (Figure 1B, C). Masson's trichrome staining demonstrated insufficient collagen synthesis and disorganized, loosely arranged collagen fibers in wounds of the model group. In contrast, ZHO treatment significantly increased collagen deposition and yielded dense, well-organized fibrous structures, thereby effectively regulating extracellular matrix remodeling during wound repair (Figure 1D). Histopathological examination showed extensive inflammatory cell infiltration and disrupted epidermal continuity in the wound tissues of db/db mice. Administration of ZHO markedly alleviated local inflammatory infiltration and facilitated ordered regeneration and structural remodeling of the epidermis (Figure 1E). Under stable blood glucose homeostasis, ZHO prominently accelerates wound healing, ameliorates the local pathological microenvironment, mitigates inflammatory damage, and promotes structural repair and remodeling of wound tissues.

3.2. Regulatory Effect of ZHO on Macrophage Polarization Phenotype and Inflammatory Microenvironment in Wounds

The results of qPCR detection of wound tissue showed that compared with the model group, ZHO could significantly down-regulate the transcription level of M1-related factors, up-regulate the expression of M2-related genes, and the regulatory effect on macrophage polarization-related genes was dose-dependent (Fig. 2A). ELISA results showed that ZHO could significantly reduce the expression of pro-inflammatory factors such as TNF-α and IL-1β in wound tissue, increase the content of anti-inflammatory factors such as IL-10 and TGF-β, and effectively balance the local inflammatory state of the wound (Fig. 2B, C). Flow cytometry results of wound tissue confirmed that after ZHO intervention, the proportion of $CD86^+$ M1 macrophages decreased significantly, and the proportion of $CD206^+$ M2 macrophages increased significantly, with a regulatory effect similar to that of the positive drug group (Fig. 2D). Immunofluorescence staining also confirmed this: the model group had a large number of $F4/80^+CD86^+$ double-positive inflammatory macrophages in the wound, while ZHO could effectively reduce the number of such cells and significantly increase the infiltration of $F4/80^+CD206^+$ reparative macrophages (Fig. 2E-H). WB results were consistent with qPCR trends: ZHO down-regulated iNOS protein expression and up-regulated Arg1 protein level, further confirming that it could induce wound macrophage polarization to M2 phenotype at the protein level (Fig. 2I). Comprehensive molecular and cellular phenotypic results showed that ZHO could effectively inhibit excessive local inflammatory response in wounds and induce macrophages to polarize from

pro-inflammatory M1 phenotype to anti-inflammatory reparative M2 phenotype.

3.3. Regulatory Mechanism of ZHO on Macrophage Polarization and CK2-βTrCP-SUN2 Protein Network

To avoid the interference of the complex microenvironment in vivo, an in vitro macrophage inflammation model was constructed in this study to explore the direct anti-inflammatory and regulatory effects of ZHO. Cell viability assay confirmed that ZHO at 1 μM began to exert cytotoxicity (Fig. 3A). Accordingly, we further investigated the effects of ZHO at concentrations ranging from 0.01 μM to 1 μM on macrophages. The results showed that ZHO exerted biological effects on macrophages starting at 0.1 μM (Fig. 3B). Q-PCR and flow results showed that ZHO could significantly down-regulate the expression of M1 macrophage marker genes iNOS, CD86 and the proportion of $CD86^+$ cells, up-regulate the transcription of M2 marker genes Arg1, CD206 and the proportion of $CD206^+$ cells, effectively mediating the polarization transition of macrophages from M1 pro-inflammatory phenotype to M2 anti-inflammatory phenotype (Fig. 3C-E). Previous studies have confirmed that the CK2-βTrCP-SUN2 signaling axis can participate in the regulation of M1/M2 polarization phenotype transition of macrophages by regulating the remodeling of macrophage nuclear structure, and is an important regulatory pathway for macrophage inflammatory response [14,22]. To reveal the potential molecular mechanism of ZHO in regulating macrophage polarization and improving inflammatory cell damage in vitro, this study further detected the protein expression changes of core factors of this pathway, and found that ZHO could significantly inhibit the expression of CK2, βTrCP, SUN1 and SUN2 core proteins (Fig. 3F). Immunofluorescence results showed that inflammatory stress could lead to nuclear shrinkage, abnormal morphology and high expression of SUN2 protein in macrophages, while ZHO intervention could effectively repair the nuclear morphology structure, reduce SUN2 protein level, and improve nuclear regularity and area (Fig. 3G-J). Notably, we observed a simultaneous reduction in the total protein levels of CK2 and βTrCP after ZHO intervention. It is worth noting that total protein abundance cannot fully reflect the functional activity of signaling molecules. We speculated that ZHO might remodel the subcellular distribution of βTrCP, facilitating the nuclear translocation of residual βTrCP protein to bind intranuclear SUN2, which could offset the decrease in total βTrCP and drive SUN2 degradation. This observation indicated that substrate binding affinity and subcellular localization, rather than total cellular protein expression, dominate the regulatory effect of the βTrCP-SUN2 axis on SUN2 homeostasis under inflammatory macrophage

conditions.

3.4. The Mediating Role of CK2-βTrCP-SUN2 Protein Network in ZHO-Regulated Macrophage Polarization

To clarify the key signaling pathway for ZHO to exert its effects, we used CK2 inhibitor CX-4945 and activator Spermidine [23] for pretreatment. the regulatory effects of ZHO on macrophage polarization markers were largely abolished; manipulation of CK2 status interfered with ZHO's ability to shift macrophage polarization phenotype (Fig. 4B). Flow cytometry results confirmed that Spermidine could counteract the effect of ZHO in reducing the proportion of $CD86^+$ cells and increasing the proportion of $CD206^+$ cells, while CX-4945 could reproduce the regulatory effect of ZHO, confirming that CK2 activity is indispensable for ZHO to modulate the βTrCP-SUN2 interaction and macrophage polarization (Fig. 4C). Western blot results showed that ZHO could significantly inhibit the protein expression of CK2, βTrCP, SUN1, SUN2 and up-regulate Arg1 level; Spermidine could reverse the down-regulation effect of ZHO on SUN2, and CX-4945 could simulate the overall regulation mode of ZHO on pathway proteins (Fig. 4D). Cellular immunofluorescence results showed that ZHO could weaken the fluorescence intensity of SUN2 and improve the nuclear shrinkage phenotype in inflammatory macrophages, Spermidine could block this effect, and CX-4945 could replicate the intervention effect of ZHO (Fig. 4E-H). Pathway intervention experiments confirmed that CK2, βTrCP and SUN2 jointly constitute a core protein network associated with ZHO-mediated regulation of macrophage polarization and nuclear morphological remodeling

3.5. Correlation between CK2/βTrCP status and ZHO-modulated SUN2 ubiquitin-proteasome degradation

To clarify the molecular mechanism of ZHO in regulating SUN2 protein expression, this study carried out verification from the levels of transcription, protein degradation and ubiquitination modification. Transcriptional verification results showed that after treatment with Actinomycin D, there was no significant difference in SUN2 mRNA levels in each group, confirming that ZHO does not regulate SUN2 expression at the transcriptional level (Fig. 5A). Protein degradation pathway screening results showed that autophagy inhibitor CQ could not reverse the down-regulation effect of ZHO on SUN2 protein, while proteasome inhibitor MG132 could significantly restore SUN2 protein content, indicating that ZHO mainly mediates SUN2 degradation through the proteasomal pathway (Fig. 5B, C). CHX chase assay results showed that ZHO

intervention could significantly shorten the half-life of SUN2 protein and accelerate its degradation (Fig. 5D). Co-IP results confirmed that ZHO could significantly enhance the ubiquitination modification level of SUN2 and promote the interaction between βTrCP and SUN2 protein; after knocking down βTrCP or inhibiting CK2 activity, the SUN2 ubiquitination and degradation process mediated by ZHO was significantly inhibited (Fig. 5E, F). Protein site mutation results showed that after SUN2 ubiquitination site mutation, the SUN2 ubiquitination and degradation effects induced by βTrCP and ZHO basically disappeared, further confirming that ZHO-induced SUN2 ubiquitination and degradation rely on intact CK2 and βTrCP protein function (Fig. 5G). Co-IP results further confirmed that ZHO markedly enhanced the binding interaction between βTrCP and SUN2, as well as the ubiquitination modification of SUN2, which appeared contradictory to the decreased total βTrCP protein detected by western blot. Combined with the above results, we proposed that ZHO does not rely on upregulating the total expression of βTrCP to promote SUN2 ubiquitination. Instead, ZHO increases the substrate affinity of remaining βTrCP toward SUN2 and promotes their colocalization in the nucleus, thereby accelerating proteasome-dependent SUN2 degradation despite the lowered overall βTrCP content.

3.6. In vivo functional verification of ZHO against infected skin wounds in diabetic db/db mice via regulating the CK2-βTrCP-SUN2 protein network

The results of in vivo pathway rescue experiments in animals showed that Spermidine could significantly weaken the effect of ZHO in accelerating wound contraction and improving healing rate, while CK2 inhibitor CX-4945 could simulate the pro-healing effect of ZHO (Fig. 6A). Flow cytometry results of wound tissue showed that Spermidine could reverse the regulatory effect of ZHO on macrophage polarization, increasing the proportion of $CD86^+$ cells and decreasing the proportion of $CD206^+$ cells, while CX-4945 could reproduce the effect of ZHO in inducing macrophage M2 polarization (Fig. 6B-D). Western blot detection results showed that Spermidine could antagonize the down-regulation effect of ZHO on CK2, βTrCP, SUN1, SUN2 proteins, and CX-4945 could replicate the regulatory characteristics of ZHO on pathway proteins (Fig. 6E). H&E and Masson staining results of wound tissue showed that after Spermidine intervention, the effects of ZHO in reducing inflammatory infiltration, promoting epidermal regeneration and increasing collagen deposition were significantly weakened, and CX-4945 could effectively replicate the repair effect of ZHO on wound tissue pathological structure and

extracellular matrix (Fig. 6F-H). In vivo rescue experiments finally confirmed that the regulatory function of ZHO on wound macrophage polarization is dependent on normal CK2 activity and functional βTrCP-SUN2 protein interaction, thereby improving the wound microenvironment and promoting wound repair.

4. Discussion

Refractory infected wounds are common complications in diabetic patients, and diabetic individuals undergoing anal fistula surgery face an extremely high risk of persistent perianal unhealed wounds due to superimposed hyperglycemia and fecal bacterial irritation, which brings huge clinical treatment difficulties. Due to their complex pathological mechanism and limited clinical efficacy. A large number of clinical and basic studies have confirmed that sustained uncontrolled inflammatory response, disordered macrophage polarization and impaired extracellular matrix reconstruction are the core links leading to delayed wound healing [24,25]. Different from normal wound repair, the wound microenvironment in wound state is in a long-term pathological state dominated by pro-inflammatory signals, and macrophages are difficult to transform to the anti-inflammatory reparative M2 phenotype, leading to slow granulation tissue growth, insufficient collagen deposition and impaired re-epithelialization [26]. This study observed that ZHO can significantly improve wound healing rate, improve tissue pathological structure and promote collagen arrangement (Fig. 1).

Macrophage polarization is a plastic biological process precisely regulated by multiple signals and pathways [27]，In addition to classic pathways such as NF-κB, STAT6, PI3K/Akt, nuclear morphology, nuclear membrane stability and mechanotransduction have also emerged as new key mechanisms regulating inflammation and polarization [28,29]. Recent studies have confirmed that the inner nuclear membrane protein SUN1/2 can maintain nuclear morphology stability by connecting nucleoskeleton and cytoskeleton, and directly participate in the regulation of macrophage polarization and inflammatory gene transcription. LPS-induced M1 polarization can significantly up-regulate SUN2 expression and cause nuclear contraction and increased nuclear stiffness, while inhibiting SUN2 can effectively reduce the release of pro-inflammatory factors [22]. This study shows that ZHO can significantly improve abnormal nuclear morphology and reduce SUN2 protein level in M1 macrophages, suggesting that nuclear membrane protein homeostasis is an important target for ZHO to exert anti-inflammatory effects (Fig. 3G-J).

Published studies have reported that CK2 kinase and E3 ligase βTrCP

cooperatively control SUN2 phosphorylation and subsequent proteasomal degradation under certain cellular contexts [22,30]. βTrCP mediates target protein ubiquitination by binding to substrate phosphorylation and degradation, and is a key molecule regulating inflammation, cycle and nuclear membrane protein homeostasis [31,32]. This study confirmed the direct interaction between βTrCP and SUN2 by Co-IP, and ZHO can significantly promote SUN2 ubiquitination, suggesting that its mechanism of action depends on protein degradation mediated by the CK2-βTrCP axis (Fig. 5).

At present, the treatment of refractory wound is still mainly anti-infection, debridement and improving microcirculation, lacking drugs targeting inflammation and polarization [33]. As a classic external prescription in traditional Chinese medicine surgery, previous studies of ZHO mostly focused on clinical efficacy and improvement of wound microenvironment [34,35]， and its molecular mechanism has not been explained from the aspects of nuclear morphology, nuclear membrane protein and ubiquitination regulation. this study firstly identifies an association between the CK2/βTrCP/SUN2 protein network and the wound-repairing efficacy of ZHO, confirming that it remodels macrophage polarization balance by regulating SUN2 ubiquitination and degradation, providing a new entry point for the study of external traditional Chinese medicine mechanism.

Our study found an apparent inconsistency that ZHO reduced total CK2 and βTrCP protein levels but strengthened βTrCP-mediated SUN2 ubiquitination and degradation. According to classic studies, CK2-dependent phosphorylation promotes βTrCP recognition and degradation of SUN2, which seems to conflict with our present protein expression data. We reasoned that the functional state of E3 ligase βTrCP is determined by multiple layers of regulation beyond total protein quantity, including subcellular trafficking, phosphorylation modification, and substrate binding affinity. Under inflammatory stimulation, most βTrCP may reside in the cytoplasm and hardly contact nuclear SUN2; ZHO treatment may promote the nuclear translocation of the limited βTrCP pool, significantly elevating the effective concentration of βTrCP around SUN2 inside the nucleus. In this scenario, even a lower total amount of βTrCP can produce stronger binding and ubiquitination effects on SUN2. Additionally, ZHO may alter the post-translational modification of βTrCP itself to improve its substrate recognition capacity, which could compensate for the reduction in total βTrCP protein. Unfortunately, the present study did not conduct further experiments to verify the nuclear-cytoplasmic distribution of βTrCP and the phosphorylation

status of βTrCP/SUN2, so the above explanations remain speculative, and more targeted validation is required in subsequent research.

In conclusion, this study verifies that ZHO simultaneously alters CK2 and βTrCP protein levels and enhances βTrCP-dependent SUN2 ubiquitination and degradation, improve abnormal nuclear morphology and regulate macrophage polarization, thereby reducing wound inflammation, promoting tissue repair and collagen deposition. The results provide experimental evidence for ZHO in the treatment of refractory wounds after anal fistula surgery, and also provide a new mechanism and target for the development of targeted drugs for chronic wounds.

5. Funding

Beijing Natural Science Foundation for Young Scholars (No. 7254495); Hebei Administration of Traditional Chinese Medicine （No.B2025056); Shanxi Province Doctoral Innovation Station（No. 2025060).

6. Conflict of interest

We all declare that we have no conflict of interest.

7. Availability of Data and Materials

All data generated or analyzed during this study are included in this published article. The raw datasets used and analyzed during the current study are available from the corresponding author on reasonable request.

8. Acknowledgment

None.

9. Author contributions

Yudong Li:Conceptualization,Funding acquisition,Project administration,Writing – review and editing,Supervision; Xue Li:Data curation,Formal analysis,Software,Investigation,Writing – original draft; Xinran Xie:Data curation,Methodology,Software; Zhongwu Zhou: Formal analysis,Validation,Software; Xiujuan He:Writing – original draft,Validation; Ling Han:Data curation,Formal analysis;Jianqiao Liu:Investigation,Validation;Yu Lu:Validation; Zihao Liu:Software;Jindong Zheng:Visualization; Yipeng Chai: Investigation.

10. References

1. Yang, H., Zhang, X. & Xue, B. New insights into the role of cellular senescence and chronic wounds. *Front. Endocrinol.* **15**, 1400462 (2024).
2. Chen, J. *et al.* Targeting matrix metalloproteases in diabetic wound healing. *Front. Immunol.* **14**, 1089001 (2023).
3. Khudhur, S. F. Hyperglycemic effects on limbs tingling and twisting sensations. *Front. Neurol.* **16**, 1591279 (2025).
4. Qin, W., Wu, Y., Liu, J., Yuan, X. & Gao, J. A Comprehensive Review of the Application of Nanoparticles in Diabetic Wound Healing: Therapeutic Potential and Future Perspectives. *Int. J. Nanomedicine* **17**, 6007–6029 (2022).
5. Deng, J., Yang, M., Zhang, X. & Zhang, H. Efficacy and safety of autologous platelet-rich plasma for diabetic foot ulcer healing: a systematic review and meta-analysis of randomized controlled trials. *J. Orthop. Surg.* **18**, 370 (2023).
6. Menter, D. G. *et al.* Platelet 'first responders' in wound response, cancer, and metastasis. *Cancer Metastasis Rev.* **36**, 199–213 (2017).
7. Lu, M. *et al.* Integrative bioinformatics analysis for identifying the mitochondrial-related gene signature associated with immune infiltration in premature ovarian insufficiency. *BMC Med.* **22**, 444 (2024).
8. Zheng, Y., Ruan, Z., Liu, S., Yang, X. & Chen, Z. Exosome-mediated macrophage polarization: Pioneering pathways in diabetic wound healing.

Int. Immunopharmacol. **161**, 115058 (2025).

9. Lu, L. *et al.* Kinsenoside-Loaded Microneedle Accelerates Diabetic Wound Healing by Reprogramming Macrophage Metabolism via Inhibiting IRE1α/XBP1 Signaling Axis. *Adv. Sci.* **12**, e2502293 (2025).
10. Yao, B. *et al.* Baihu renshen decoction ameliorates type 2 diabetes mellitus in rats through affecting gut microbiota enhancing gut permeability and inhibiting TLR4/NF-κB-mediated inflammatory response. *Front. Cell. Infect. Microbiol.* **12**, 1051962 (2022).
11. Horiguchi, M., Hata, S., Tsurudome, Y. & Ushijima, K. Characterizing the degeneration of nuclear membrane and mitochondria of adipose-derived mesenchymal stem cells from patients with type II diabetes. *J. Cell. Mol. Med.* **25**, 4298–4306 (2021).
12. Hu, S., Qu, X., Jiao, Y., Hu, J. & Wang, B. Immune Classification and Immune Landscape Analysis of Triple-Negative Breast Cancer. *Front. Genet.* **12**, 710534 (2021).
13. Jiao, S. *et al.* SUN1/2 controls macrophage polarization via modulating nuclear size and stiffness. *Nat. Commun.* **14**, 6416 (2023).
14. Krshnan, L. *et al.* Regulated degradation of the inner nuclear membrane protein SUN2 maintains nuclear envelope architecture and function. *eLife* **11**, e81573 (2022).
15. Bulanova, D. *et al.* A synthetic lethal dependency on casein kinase 2 in response to replication-perturbing therapeutics in RB1-deficient cancer

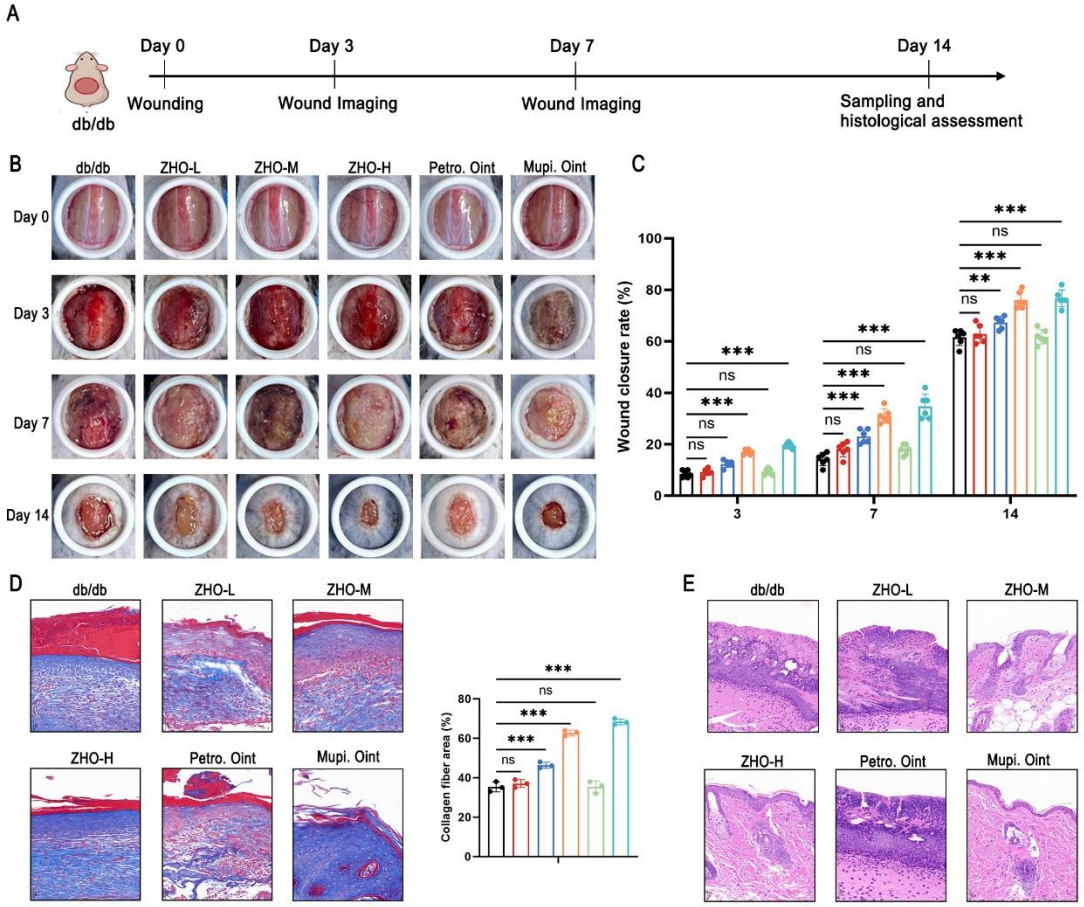
cells. *Sci. Adv.* **10**, eadj1564 (2024).

16. Wang, L. *et al.* [Effect of zhuhong ointment on renal antioxidant capability in skin ulcer model rats]. *Zhongguo Zhong Yao Za Zhi Zhongguo Zhongyao Zazhi China J. Chin. Mater. Medica* **37**, 735–738 (2012).
17. Wang, GY *et al.* Clinical safety study of Zhuhong Ointment in the treatment of chronic skin ulcers. *Beijing J. Tradit. Chin. Med.* **35**, 70–72 (2016).
18. Xiaoli Kong & Xuying Xu. Clinical study on mercury concentration fluctuations in blood and urine during Zhuhong Ointment treatment for chronic skin ulcers. *West. J. Tradit. Chin. Med.* **30**, 79–82 (2017).
19. Xiaoye Wang. Toxicological Study on Transdermal Absorption of Mercury Components in External Mineral Medicine Zhuhong Ointment. (Beijing University of Chinese Medicine, 2018). doi:10.26973/d.cnki.gbjzu.2018.000247.
20. Xiaobin Fu & Dewen Wang. *Fundamentals of Wound Repair*. (1997).
21. Xiaojian Sun, Mengyue Zhao, Hongchang Wang, & Xiyun Mao. Effect of Baijie San on the expression of ICAM-1 and TNF-α in a rat model of acute infectious wounds after anal fistula surgery. *Chin. J. Emerg. Tradit. Chin. Med.* **31**, 974–977 (2022).
22. Jiao, S. *et al.* SUN1/2 controls macrophage polarization via modulating nuclear size and stiffness. *Nat. Commun.* **14**, 6416 (2023).
23. Li, R. *et al.* Polyamines protect porcine sperm from lipopolysaccharide-induced mitochondrial dysfunction and apoptosis via casein kinase 2

546 activation. *J. Anim. Sci.* **103**, skae383 (2025).
547 24. Fan, Y., Lin, Z., Cheng, L. & Ge, L. Levels of peripheral CD4 + and CD8 + T
548 cells and glycaemic control level in patients with both type 2 mellitus
549 diabetes and stage III-IV periodontitis: a randomized controlled trial in
550 Chinese population. *BMC Oral Health* **25**, 1065 (2025).
551 25. Wang, S., Cheng, W., Wang, X., Wu, Z. & Su, J. Progress of microneedle
552 targeted modulation technology in the reconstruction of immune
553 microenvironment in diabetic wounds. *Eur. J. Med. Res.* **30**, 405 (2025).
554 26. Lu, L. *et al.* Kinsenoside-Loaded Microneedle Accelerates Diabetic Wound
555 Healing by Reprogramming Macrophage Metabolism via Inhibiting
556 IRE1α/XBP1 Signaling Axis. *Adv. Sci.* **12**, e2502293 (2025).
557 27. Wang, S., Liu, G., Li, Y. & Pan, Y. Metabolic Reprogramming Induces
558 Macrophage Polarization in the Tumor Microenvironment. *Front. Immunol.*
559 **13**, 840029 (2022).
560 28. Jong, Y.-J. I. & O'Malley, K. L. Functional G protein-coupled receptors on
561 nuclei from brain and primary cultured neurons. *Methods Mol. Biol.* **1234**,
562 113–121 (2015).
563 29. Li, Y. & Alam, H. B. Creating a pro-survival and anti-inflammatory phenotype
564 by modulation of acetylation in models of hemorrhagic and septic shock.
565 *Adv. Exp. Med. Biol.* **710**, 107–133 (2012).
566 30. Semplici, F., Meggio, F., Pinna, L. A. & Oliviero, S. CK2-dependent
567 phosphorylation of the E2 ubiquitin conjugating enzyme UBC3B induces its

interaction with beta-TrCP and enhances beta-catenin degradation. *Oncogene* **21**, 3978–3987 (2002).

31. Li, J. *et al.* SelK promotes glioblastoma cell proliferation by inhibiting β-TrCP1 mediated ubiquitin-dependent degradation of CDK4. *J. Exp. Clin. Cancer Res. CR* **43**, 231 (2024).
32. Liu, J. *et al.* SDCBP promotes pancreatic cancer progression by preventing YAP1 from β-TrCP-mediated proteasomal degradation. *Gut* **72**, 1722–1737 (2023).
33. Wan, X. *et al.* Research progress and application prospect of adipose-derived stem cell secretome in diabetes foot ulcers healing. *Stem Cell Res. Ther.* **15**, 279 (2024).
34. Huike Ma *et al.* Effect of Zhuhong Ointment on neutrophil extracellular traps in diabetic foot ulcer wounds. *Lishizhen Med. Mater. Medica Res.* **36**, 2104–2108 (2025).
35. Zhongwu Zhou *et al.* Clinical study of Zhuhong Ointment gauze in promoting postoperative wound healing of low simple anal fistula. *J. Colorectal Anal Surg.* **27**, 585–588 (2021).



586

587 Fig1. ZHO Improves Pathological Damage and Accelerates Wound Healing in
588 db/db Mice. (A) Schematic diagram of the experimental protocol; (B)
589 Representative photographs of wounds in each group on days 0, 3, 7 and 14
590 after modeling; (C) Statistical results of wound healing rate in each group on
591 days 3, 7, and 14 after modeling; (D) Representative images and quantitative
592 analysis of Masson trichrome staining of wounds in each group on day 14 after
593 modeling(40X); (E) Representative images of H&E staining of wounds in each
594 group on day 14 after modeling(40X). Data are presented as mean ± standard
595 deviation. *p<0.05, ***p<0.001; ns, no significant difference, n≥3.

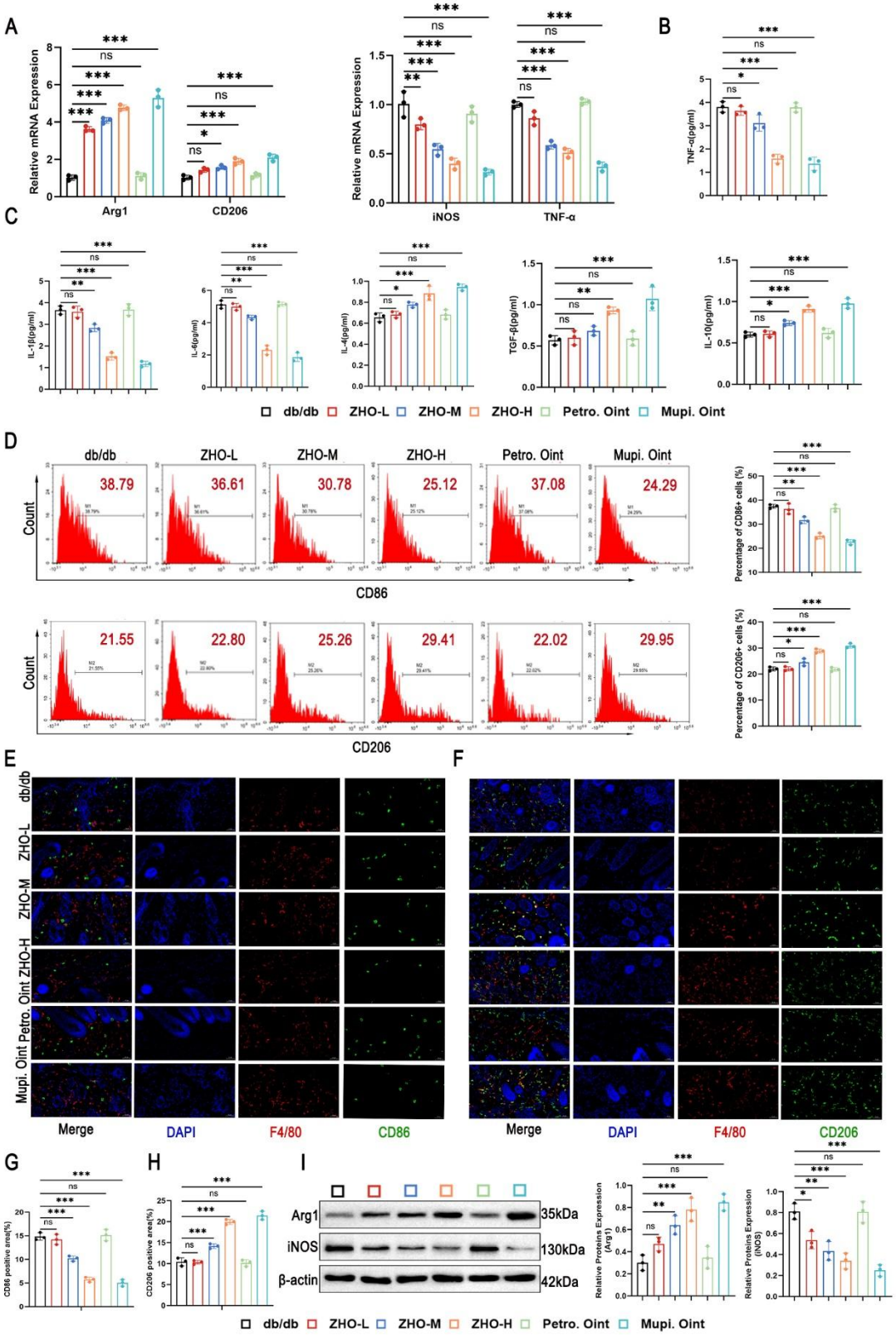


Fig2. Regulatory Effect of ZHO on Macrophage Polarization Phenotype and Inflammatory Microenvironment in Wounds. (A) mRNA expression levels of macrophage polarization-related marker genes in wound tissues; (B) Detection results of pro-inflammatory factor TNF-α content in wound tissues; (C)

Detection results of M1 and M2 phenotype-related factor contents in wound tissues; (D) Flow cytometric analysis results of macrophages in wound tissues; (E)(G) Representative images and quantitative analysis of F4/80^{+}CD86^{+} immunofluorescence staining in wound tissues; (F)(H) Representative images and quantitative analysis of F4/80^{+}CD206^{+} immunofluorescence staining in wound tissues; (I) Protein expression levels of iNOS and Arg1 in wound tissues. Data are presented as mean ± standard deviation. *p<0.05, ***p<0.001; ns, no significant difference.

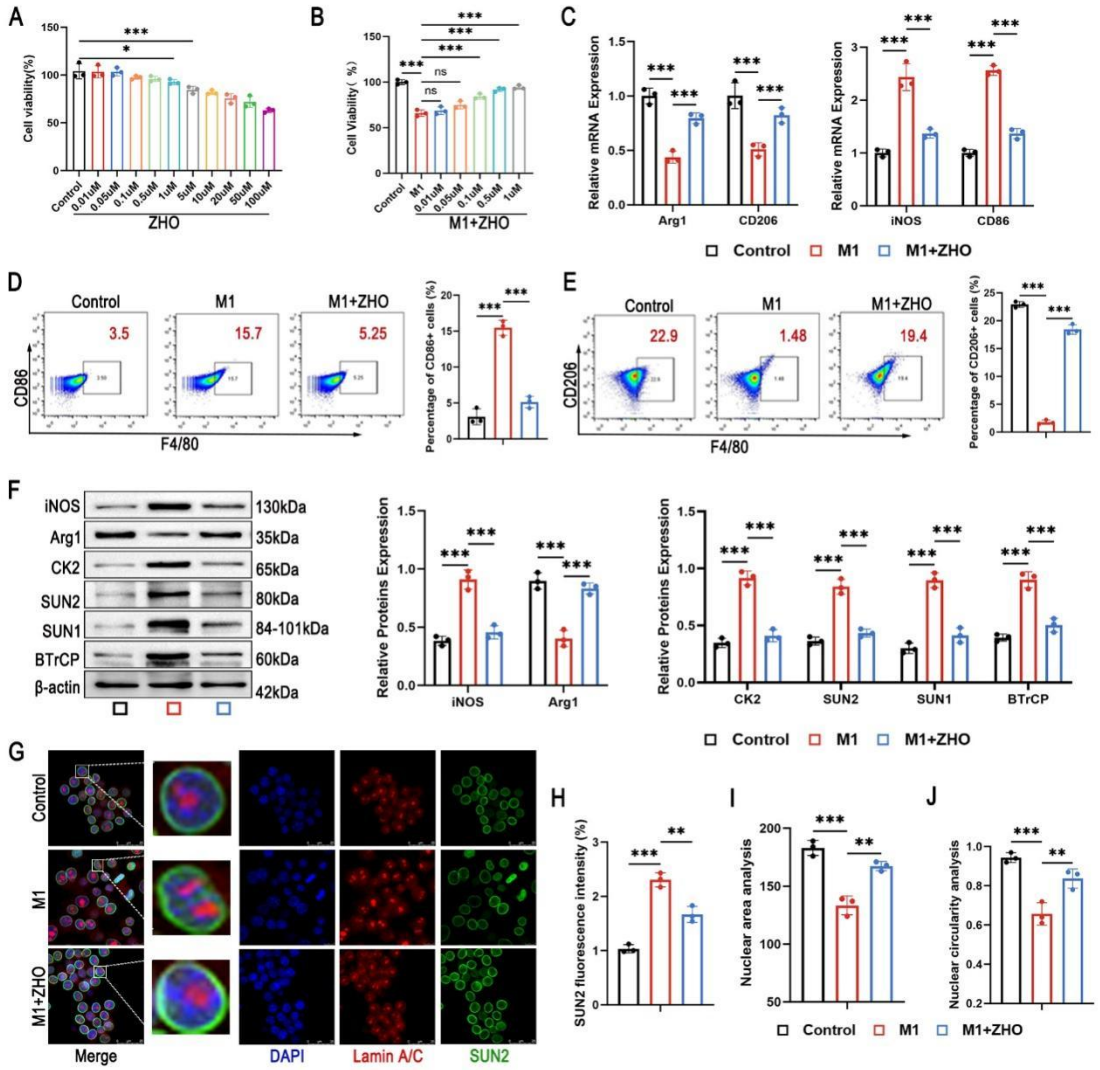


Fig3. Regulatory Mechanism of ZHO on Macrophage Polarization and CK2-βTrCP-SUN2 Protein Network. (A) Effect of ZHO on cell viability detected by CCK-8 assay; (B) Screening of the effective concentration of ZHO on macrophages detected by CCK-8 assay; (C) mRNA expression levels of M1 and M2 markers in macrophages detected by qRT-PCR; (D) Expression

proportion and quantitative analysis of CD86 on the surface of macrophages in each group detected by flow cytometry; (E) Expression proportion and quantitative analysis of CD206 on the surface of macrophages in each group detected by flow cytometry; (F) Protein expression levels and quantitative gray analysis in macrophages of each group detected by Western blot; (G) Representative immunofluorescence images of Lamin A/C (green) and SUN2 (red) in macrophages of each group detected by confocal microscopy; (H) Mean fluorescence intensity of SUN2; (I) Nuclear area; (J) Nuclear circularity analysis. Data are presented as mean ± standard deviation (n=3). *p<0.05, **p<0.01, ***p<0.001.

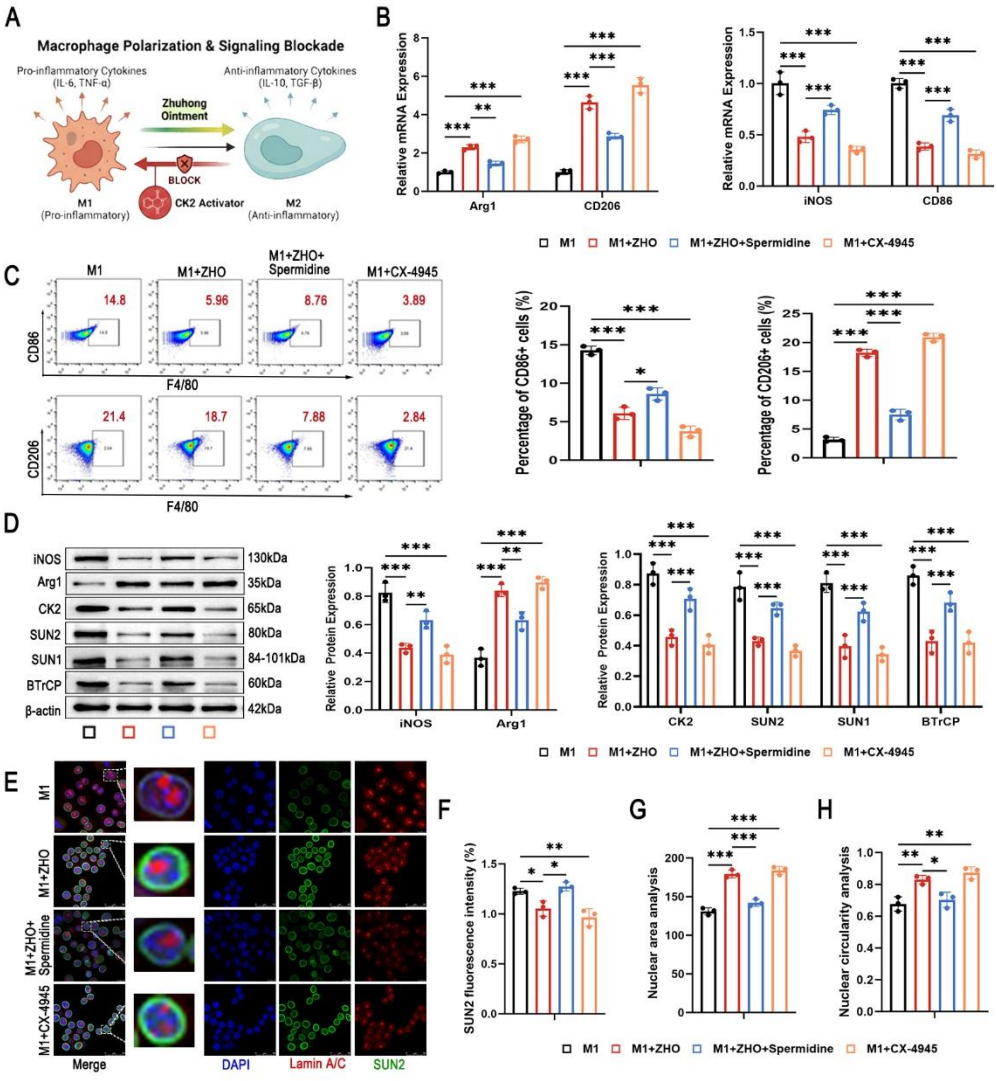


Fig4. The Mediating Role of CK2-βTrCP-SUN2 Protein Network in ZHO-Regulated Macrophage Polarization. (A) Schematic diagram of the mechanism of ZHO; (B) mRNA expression levels of M1 and M2 markers in macrophages of each group detected by qRT-PCR; (C) Expression proportions

and quantitative analysis of CD86 and CD206 on the surface of macrophages in each group detected by flow cytometry; (D) Protein expression levels and quantitative gray analysis in macrophages of each group detected by Western blot; (E) Representative immunofluorescence images of Lamin A/C (green) and SUN2 (red) in macrophages of each group detected by confocal microscopy; (F) Mean fluorescence intensity of SUN2; (G) Nuclear area; (H) Nuclear circularity analysis. Data are presented as mean ± standard deviation (n=3). *p<0.05, **p<0.01, ***p<0.001.

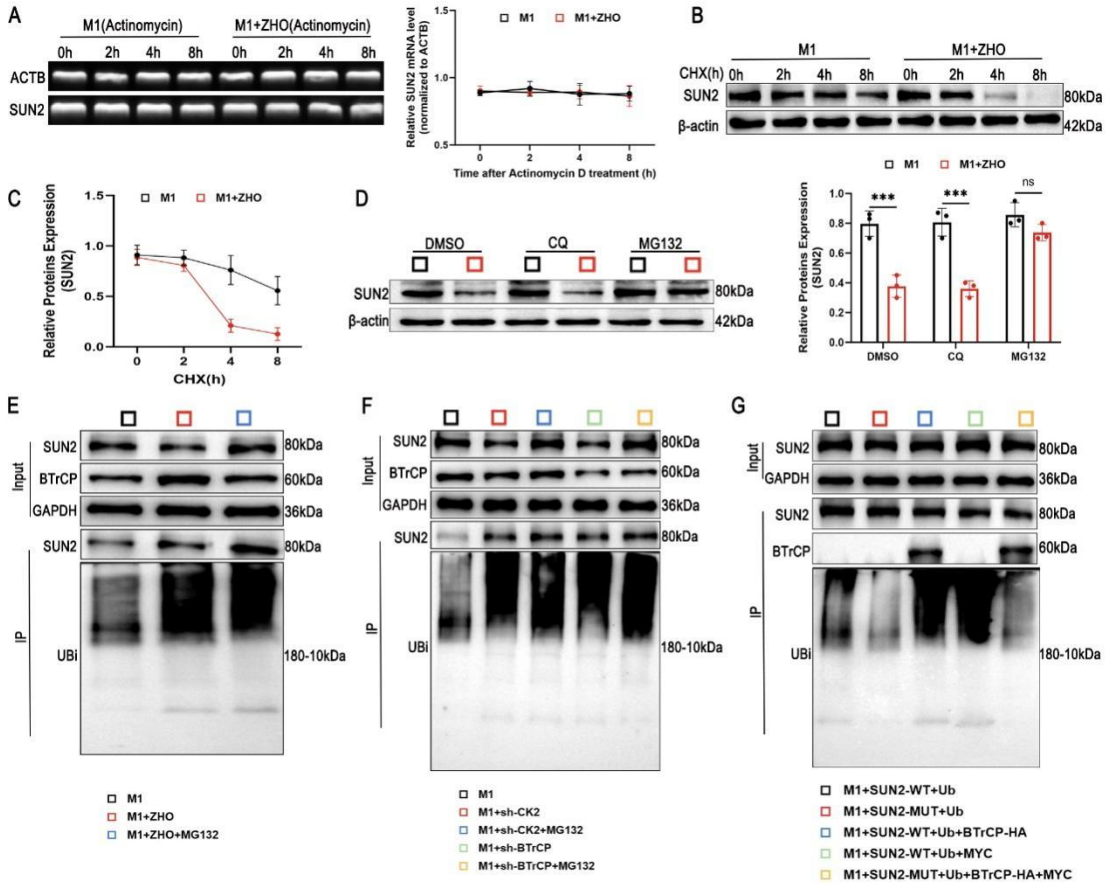


Fig5. Correlation between CK2/βTrCP status and ZHO-modulated SUN2 ubiquitin-proteasome degradation. (A) Stability assay of SUN2 mRNA in macrophages under Actinomycin D treatment; (B-C) SUN2 protein changes in macrophages detected by CHX chase assay; (D) Western blot analysis of SUN2 protein expression levels and quantitative gray analysis after CQ or

MG132 treatment; (E-F) SUN2 ubiquitination level and binding ability between SUN2 and βTrCP detected by co-immunoprecipitation assay; (G) Protein degradation after mutation of SUN2 ubiquitination sites. Data are presented as mean ± standard deviation (n=3). *p<0.05, **p<0.01, ***p<0.001.

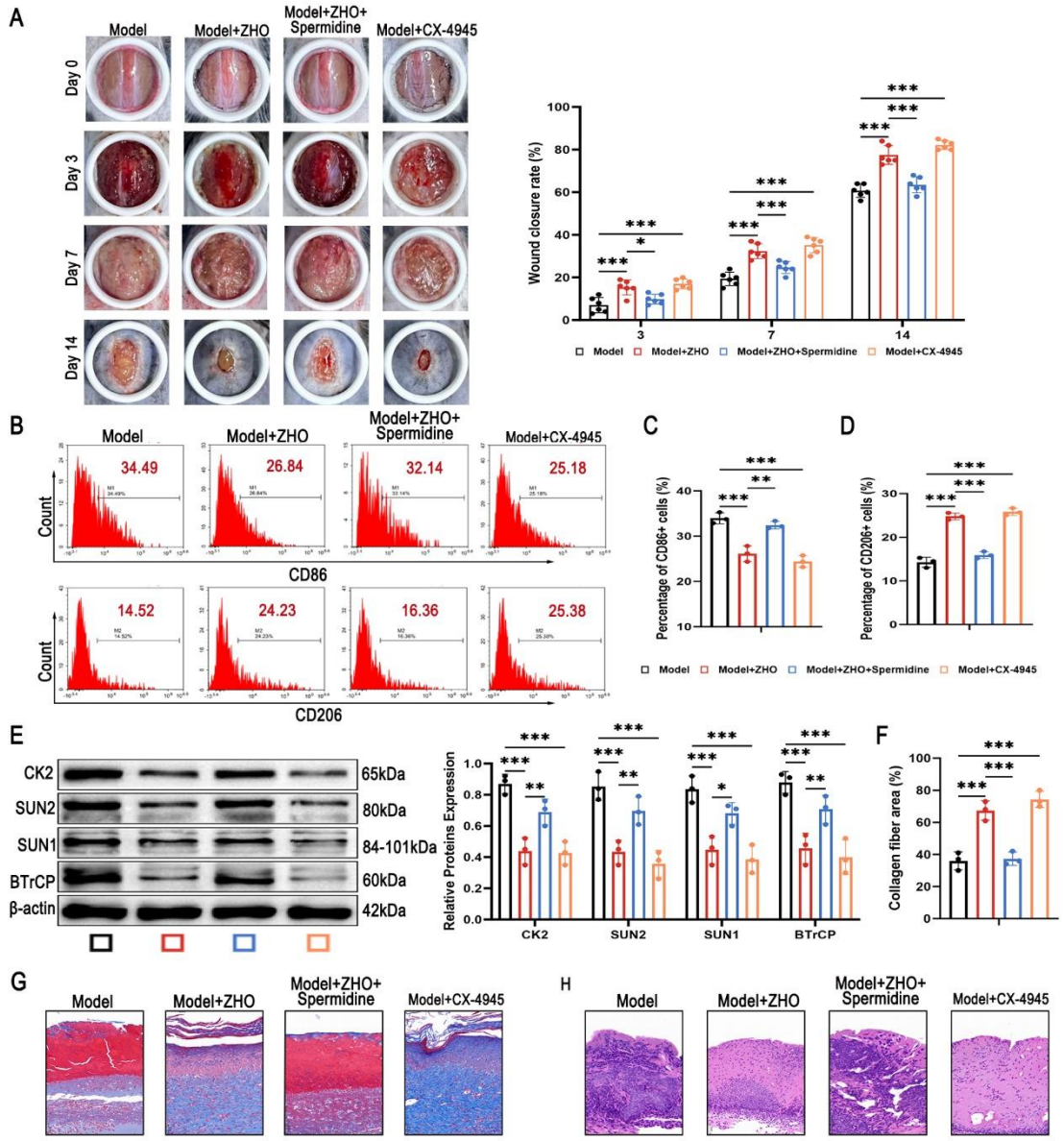


Fig6. In vivo functional verification of ZHO against infected skin wounds in diabetic db/db mice via regulating the CK2-βTrCP-SUN2 protein network. (A) Representative photographs of wounds and statistical analysis of wound healing rate in each group on days 0, 3, and 14 after in vivo pathway intervention (n=6); (B-D) Flow cytometric results of wound macrophages after in vivo pathway intervention; (E) Expression levels of proteins related to the CK2-βTrCP-SUN protein network and macrophage polarization in wound tissues; (F-G) Quantitative analysis and representative images of Masson's

trichrome staining in each group on day 14 after modeling; (H) Representative images of H&E staining. Data are presented as mean ± standard deviation. *p<0.05, ***p<0.001; ns, no significant difference.

Supplementary Files

This is a list of supplementary files associated with this preprint. Click to download.

- GraphicalAbstract.jpg